A Novel Fast and Reduced Redundancy Structure for Multiscale Directional Filter Banks

Kin-On Cheng, Ngai-Fong Law, *Member, IEEE*, and Wan-Chi Siu, *Senior Member, IEEE*

***Abstract*—The multiscale directional filter bank (MDFB) improves the radial frequency resolution of the contourlet transform by introducing an additional decomposition in the high-frequency band. The increase in frequency resolution is particularly useful for texture description because of the quasi-periodic property of textures. However, the MDFB needs an extra set of scale and directional decomposition, which is performed on the full image size. The rise in computational complexity is, thus, prominent. In this paper, we develop an efficient implementation framework for the MDFB. In the new framework, directional decomposition on the first two scales is performed prior to the scale decomposition. This allows sharing of directional decomposition among the two scales and, hence, reduces the computational complexity significantly. Based on this framework, two fast implementations of the MDFB are proposed. The first one can maintain the same flexibility in directional selectivity in the first two scales while the other has the same redundancy ratio as the contourlet transform. Experimental results show that the first and the second schemes can reduce the computational time by 33.3%–34.6% and 37.1%–37.5%, respectively, compared to the original MDFB algorithm. Meanwhile, the texture retrieval performance of the proposed algorithms is more or less the same as the original MDFB approach which outperforms the steerable pyramid and the contourlet transform approaches.**

***Index Terms*—Fast algorithm, multidirection, multiscale, multiscale directional filter bank (MDFB), texture retrieval.**

I. Introduction

In the past decades, various filter bank-related techniques have been developed for image processing tasks such as texture retrieval, segmentation, image compression, denoising, enhancement, etc. Their corresponding basis functions or frames are often localized in spatial and frequency domain so as to provide an efficient representation of natural images. Some popular filter bank approaches include wavelet transform [1], Gabor wavelets [2], [3], steerable pyramids [4]–[6], and contourlet transform [7], [8].

The standard 2-D wavelet transform possesses multiresolution and maximum decimation properties. However, the wavelets have limited directional sensitivity due to its separable nature so it is not very effective in edge representation. Recently, several direction-adaptive approaches [9]–[11] based on wavelet transform have been proposed so as to provide a sparse representation of images with edges. In bandelets [9] and directionlets [10], 1-D wavelet transform is applied to the orientations of local directional features of images. In [11], directional lifting [12] is performed adaptively by selecting an appropriate direction from a set of candidates. Their adaptive nature leads to high compression ratio but this may incur difficulty in image comparison. Furthermore, these algorithms usually involve extra operations for direction selection.

Gabor wavelets, steerable pyramids and the contourlet transform provide a nonadaptive representation of image with high flexibility in orientation decomposition but the representation is over-complete. In the contourlet transform, the Laplacian pyramid (LP) [13], [14] is used for multiscale decomposition while the directional filter bank (DFB) [15] is employed for directional decomposition. Since the DFB is maximally decimated, the contourlet transform has lower redundancy and computational complexity than the Gabor wavelets and steerable pyramids. It has been shown that the contourlets can achieve the same asymptotic rate of decay in reconstruction error as curvelets [16]. Therefore, the contourlet transform is suitable for image compression as well as image comparison and analysis. On the other hand, the decimation in the DFB as well as in the LP introduces aliasing in the subband domain. It has been pointed out that the aliasing problem would deteriorate the directional sensitivity [17] and shift invariant property [5]. The aliasing, however, can be alleviated by requiring the lowpass filter used in scale decomposition to have stopband edge at or below $\pi/2$. The adverse effect of the stopband edge constraint is the reduction of frequency resolution in high and mid radial frequency bands.

In [18] and [19], we proposed the multiscale directional filter bank (MDFB) to improve the radial frequency resolution in the contourlet transform by splitting the highest frequency band in the LP into two frequency bands. Besides compensating the adverse effect of the nonaliasing requirement in the LP, the increase in resolution of high and mid-frequency range is particular useful for texture characterization. Our previous works have shown that the MDFB has better performance in texture retrieval than the steerable pyramid and comparable to the Gabor wavelet. Since no decimation is performed in the new scales, the MDFB has higher redundancy than the contourlet transform.

The framework of the original MDFB follows the steerable pyramid and the contourlet transform that all the multiscale decomposition is performed prior to the directional decomposition. In this paper, we propose two fast versions of the MDFB by

Manuscript received October 20, 2006; revised April 20, 2007. This work was supported in part by the Centre for Signal Processing, Department of Electronic and Information Engineering, The Hong Kong Polytechnic University, and in part by CERG under Grant PolyU 5222/03E of the Hong Kong SAR Government. The associate editor coordinating the review of this manuscript and approving it for publication was Dr. Pier Luigi Dragotti.

The authors are with the Centre for Signal Processing, Department of Electronic and Information Engineering, The Hong Kong Polytechnic University, Hong Kong (e-mail: k.o.cheng@polyu.edu.hk; ennflaw@polyu.edu.hk; enwcsiu@polyu.edu.hk).

Color versions of one or more of the figures in this paper are available online at http://ieeexplore.ieee.org.

Digital Object Identifier 10.1109/TIP.2007.901212

swapping the two processes, i.e., scale and directional decomposition in the first two scales. In the first scheme, each directional subband in the first level of the LP is split into two frequency bands of different radial frequency ranges by lowpass filtering and subtraction. It has the same flexibility as the original MDFB that different scales can have different directional selectivity, but the saving in computational complexity can be more than 33%. In the second scheme, the scale decomposition of directional subbands is implemented using a wavelet-like transform. Similar reduction in computational complexity to the first approach can be achieved. Although due to decimation, directional decomposition is required to be the same in the first two scales, the resultant MDFB has the same redundancy as the contourlet transform, i.e., redundancy ratio $= 4/3$.

This paper is organized as follows. In Section II, we give background on the MDFB. In Section III, scale decomposition in directional subbands is first analyzed. From the analysis, we find that the contourlet subbands can be further split into finer scales. Two methods have been developed to split the contourlet subbands into two different scales. One method uses lowpass filtering and subtraction. Another method employs a wavelet-like transform. In Section IV, we adopt the proposed splitting schemes to implement two fast algorithms of the MDFB. We also discuss the filter designs for the new algorithms and estimate the computational complexity using the number of arithmetic operations. Section V presents experimental results on the computational time and texture retrieval performance of our proposed algorithms. The results are also compared with those based on the original algorithm and the contourlet transform. Finally, we conclude the paper in Section VI.

II. Background

A. Laplacian Pyramid

The Laplacian pyramid (LP) [13] is an overcomplete decomposition in which an input image is represented by a set of bandpass images and a lowpass image. Ideally, the ith bandpass image represents components in frequency range $[-\pi/2^{i-1}, \pi/2^{i-1}]^2 \setminus [-\pi/2^i, \pi/2^i]^2$ where $i = 1, 2, \ldots, N$ and N is the number of decomposition levels. A lowpass image contains frequency components in $[-\pi/2^N, \pi/2^N]^2$. In the LP, the input image is first processed by a lowpass filter $h_L^{2-D}[\mathbf{n}]$ and a downsampler to generate a lowpass image. A coarse prediction of the original image is computed by upsampling and subsequently convolving the lowpass image using another lowpass filter $g_L^{2-D}[\mathbf{n}]$. By subtracting the coarse prediction from the input signal, a bandpass image is obtained. The process can be iterated on the lowpass image to generate other bandpass images in lower frequency range. A block diagram of this iterative process is shown in Fig. 1. In this paper, we set $g_L^{2-D}[\mathbf{n}]$ to be the time reverse version of $h_L^{2-D}[\mathbf{n}]$, i.e., $g_L^{2-D}[\mathbf{n}] = h_L^{2-D}[-\mathbf{n}]$ for convenience. In addition, $h_L^{2-D}[\mathbf{n}]$ is realized using separable filtering with a 1-D filter $h_L[n]$. The main feature of the LP is that decimation is performed only on the lowpass image. Thus, there is no frequency scrambling. Further processing such as directional decomposition can be performed directly on the bandpass images [7], [8].

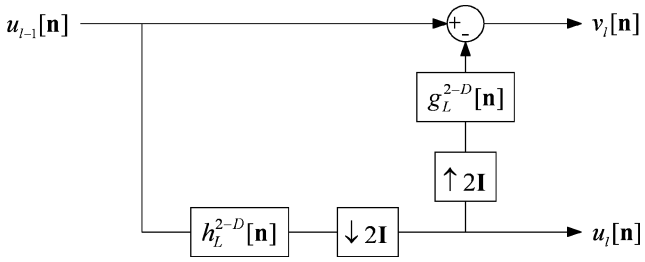

Fig. 1. Iterative structure of the LP.

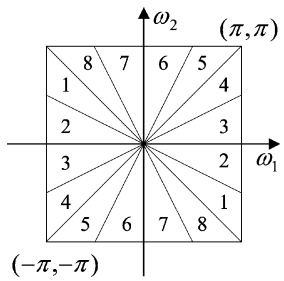

Fig. 2. Partitioning of the frequency plane in a three-level DFB.

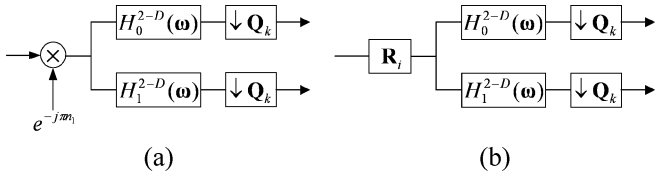

Fig. 3. Building blocks of the DFB (a) type I and (b) type II. In the figures, $H_0^{2-D}(\boldsymbol{\omega})$ and $H_1^{2-D}(\boldsymbol{\omega})$ are complementary diamond-shaped filters. $\mathbf{Q}_k$ and $\mathbf{R}_i$ are a quincunx downsampling matrix and a resampling matrix, respectively.

B. Directional Filter Bank

Directional filter bank (DFB) was originally proposed in [15] as a critically sampled directional decomposition. The DFB partitions a frequency plane into a set of wedge-shape region as illustrated in Fig. 2. It can be implemented efficiently in a tree structure using two types of building blocks as shown in Fig. 3. Both types of building blocks rely on a two-channel filter bank in which a complementary diamond-shaped filter pair is followed by a quincunx downsampling. In the type I building block, modulation is performed prior to the two-channel filter bank so that fan-shaped partitions are generated. In the type II building block, the modulator is replaced by a resampler. Its function is to shear the desired frequency partitions into diamond shape so that the two-channel filter bank can give the desired frequency bands. Because of sampling, subbands would suffer from spatial distortion [20], [21]. The problem can be solved by adopting backsampling at the output of the DFB. The backsampling reorders the subbands so that the overall sampling is diagonal. For subband s, the overall sampling matrix $\mathbf{M}_s$ is given by

$$\mathbf{M}_s = \begin{cases} 2\mathbf{D}_1^{i-2}, & s \text{ in } \Re_0 \\ 2\mathbf{D}_0^{i-2}, & s \text{ in } \Re_1 \end{cases} \tag{1}$$

where $i (i \geq 2)$ is the index of output stage of DFB, $\Re_j$, $j = 0, 1$ are spectral regions defined in Fig. 4 and downsampling

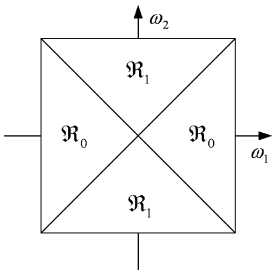

Fig. 4. Definition of frequency regions $\Re_j$, $j = 0, 1$.

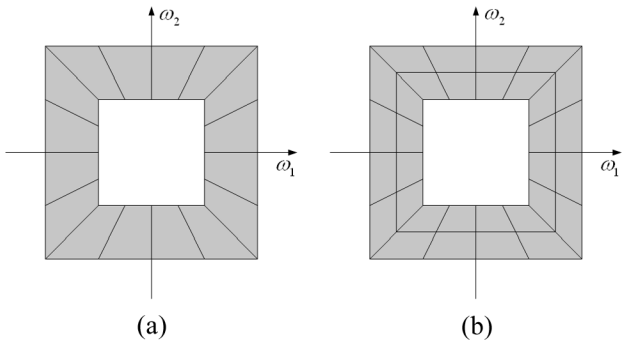

Fig. 5. Spectrum decomposition in frequency $[-\pi, \pi]^2 \setminus [-\pi/2, \pi/2]^2$ for (a) the contourlet transform and (b) the MDFB.

matrices $\mathbf{D}_0$ and $\mathbf{D}_1$ are defined by $\mathbf{D}_0 = \begin{bmatrix} 2 & 0 \\ 0 & 1 \end{bmatrix}$ and $\mathbf{D}_1 = \begin{bmatrix} 1 & 0 \\ 0 & 2 \end{bmatrix}$, respectively.

C. Multiscale DFB

The multiscale DFB (MDFB) [18] modifies the pyramidal directional filter bank (PDFB) or the contourlet transform by splitting the finest scale in frequency $[-\pi, \pi]^2 \setminus [-\pi/2, \pi/2]^2$ into two scales in frequency $[-\pi, \pi]^2 \setminus [-3\pi/4, 3\pi/4]^2$ and $[-3\pi/4, 3\pi/4]^2 \setminus [-\pi/2, \pi/2]^2$. The scale decomposition of the MDFB is achieved by first applying a lowpass filter of cutoff frequency at 0.75π to an input image. The lowpass image is subtracted from the input image to generate the first scale. The LP is then applied on the lowpass image. The second scale is obtained as the first bandpass image in the LP. The third scale is the second bandpass image in the LP, and so on. After that, the DFB is applied separately on each bandpass image. Fig. 5 compares the decomposition of the contourlet transform and the MDFB in the frequency $[-\pi, \pi]^2 \setminus [-\pi/2, \pi/2]^2$. As seen, the decomposition of the finest bandpass image increases the frequency resolution at high and mid-frequency range. It has been shown that this can improve the texture description [18], [19] because texture images have quasi-periodic patterns [22]. As a result, [19] shows that the MDFB outperforms steerable pyramid in texture retrieval. As mentioned in [17], the lowpass filter used in the LP should have stopband edge at or below $\pi/2$ to avoid aliasing, which would cause reduction in angular resolution. For nonideal filters, it requires lowering the cutoff frequency of the lowpass filter below $\pi/2$, and so this decreases the resolution at the high-frequency subband. Therefore, the additional decomposition of the finest bandpass image can compensate the adverse effect of nonaliasing filters, as well [19].

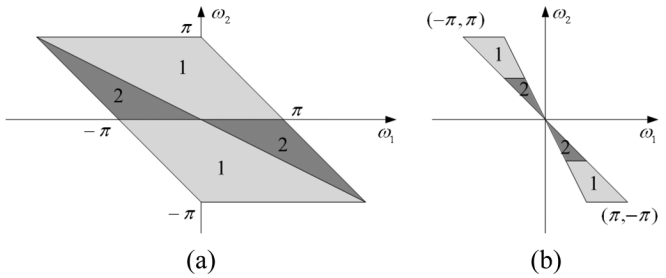

Fig. 6. Ideal spectrum of directional subband "8" in Fig. 2: (a) in the subband domain and (b) in the input domain with backsampling. In the figures, the high-frequency and low-frequency regions in the input domain are denoted respectively by light and dark colors.

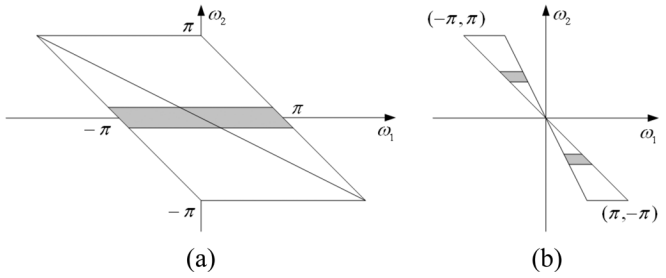

Fig. 7. (a) Lowpass filtered directional subband and (b) the equivalent frequency response of the filtered subband in (a) at the input of the DFB.

III. Additional Scale Decomposition in a Contourlet Subband

As mentioned in Section II-C, the MDFB splits the first scale of the contourlet transform into two scales. Actually, the additional scale decomposition for the first scale can be applied on other scales and vice versa. In this section, we develop two efficient additional scale decomposition schemes suitable for any bandpass scale of the contourlet transform. At first, analysis on scale decomposition in directional subbands is presented. Based on the analysis, we propose two subband decomposition schemes, namely, the lowpass filtering approach and the wavelet-like decomposition approach.

A. Analysis of Scale Decomposition in Directional Subbands

In our proposed algorithms, further scale decomposition is performed after the DFBs. Given a DFB with two or more levels and without loss of generality, consider a directional subband in a three-level DFB, which corresponds to a frequency region shown in Fig. 6(b). Because of modulation and sampling, subbands of the DFB suffer from frequency scrambling which translates the low-frequency components to high-frequency regions as indicated in Fig. 6(a). If a vertical bandpass filter is applied to extract frequency components corresponding to a scale in region 1, it is inevitable to mix with frequency components in region 2. Similar situation occurs for filtering in region 2. The extraction is different for a lowpass filter. As demonstrated in Fig. 7, a scale can be obtained without mixing with other scales because scrambled frequency components

across the DC line belong to the frequency region. Unfortunately, this is limited to only one mid-frequency region. In fact, delicate nonseparable filters are required to have flexible scale decomposition. However, the situation is simplified if either region 1 or region 2 is removed. Apart from the lowpass subband, we always have the scenario that region 2 is removed as a by-product in the contourlets. Hence, the bandpass contourlets can be split using the simple bandpass filtering. For another scenario that region 1 is removed, the bandpass filtering scheme can be used to obtain the coarser scale components. However, the overall scheme is not as effective as the contourlet transform because in order to obtain the second scenario, downsampling cannot be performed on the lowpass residual in the first scale decomposition. This increases the computational complexity in the subsequent directional decomposition and scaling decomposition, as well as overall redundancy. Therefore, we focus on the splitting of the bandpass contourlets. In particular, each scale of the contourlet transform is split into two scales despite that the number of split scales can be more. We will see that the proposed splitting schemes can be used to obtain fast algorithms for the MDFB.

B. Splitting Based on Lowpass Filtering

Suppose that a directional subband $s[\mathbf{n}]$ of the DFB is in spectral region $\Re_1$ defined in Fig. 4. We apply a 2-D lowpass vertical filter $h_c^{2-D}[\mathbf{n}]$ to extract the lower frequency band, $c[\mathbf{n}]$. The higher frequency band $d[\mathbf{n}]$ is obtained by subtracting the lower frequency band from the directional subband. Mathematically, $c[\mathbf{n}]$ and $d[\mathbf{n}]$ are generated by

$$c[\mathbf{n}] = \sum_{k\in Z^2} s[\mathbf{k}] h_c^{2-D}[\mathbf{n}-\mathbf{k}] \tag{2}$$

$$d[\mathbf{n}] = s[\mathbf{n}] - c[\mathbf{n}]. \tag{3}$$

With backsampling, the overall sampling of stage i after the second stage is a downsampler in the horizontal direction $\mathbf{D}_0^{i-2}$. Using noble identity [23], the corresponding filter response just after the second stage is the same as the upsampled vertical filter $H_{uc}^{2-D}(\boldsymbol{\omega})$ given by

$$H_{uc}^{2-D}(\boldsymbol{\omega}) = H_c^{2-D}\left(\left(\mathbf{D}_0^{i-2}\right)^T \boldsymbol{\omega}\right) = H_c^{2-D}\left(\mathbf{D}_0^{i-2}\boldsymbol{\omega}\right). \tag{4}$$

Using noble identity and demodulation, it can be shown that $H_{uc}^{2-D}(\boldsymbol{\omega})$ is related to a filter at the input of the DFB $H_{bc}^{2-D}(\boldsymbol{\omega})$ by

$$H_{bc}^{2-D}(\boldsymbol{\omega}) = H_{uc}^{2-D}(2\boldsymbol{\omega} - \mathbf{p}) \tag{5}$$

where $\mathbf{p} = [\pi, \pi]^T$ is the frequency shift due to the modulation in the first two stages. Substituting (4) into (5), we have

$$\begin{aligned} H_{bc}^{2-D}(\boldsymbol{\omega}) &= H_c^{2-D}\left(\mathbf{D}_0^{i-2}(2\boldsymbol{\omega} - \mathbf{p})\right) \\ &= \begin{cases} H_c^{2-D}(2\omega_1 - \pi, 2\omega_2 - \pi), & i = 2 \\ H_c^{2-D}(2^{i-1}\omega_1, 2\omega_2 - \pi), & i > 2 \end{cases}. \end{aligned} \tag{6}$$

Here, the 2π-periodic property of spectrum is used in the case of $i > 2$. Using (6), it can be verified that a vertical lowpass filter in the subband domain illustrated in Fig. 8(a) is equivalent to a bandpass filter with centre frequency at $\omega_2 = \pi/2$ described in Fig. 8(b). For the highpass channel, the equivalent response consists of two passbands centred at $\omega_2 = 0$ and $\omega_2 = \pi$. The spectra of outputs $\mathrm{c}[\mathbf{n}]$ and $\mathrm{d}[\mathbf{n}]$ are, thus, given as in Figs. 9 and 10, respectively. For directional subbands in spectral region $\Re_0$, the roles of ω_1 and ω_2 are interchanged. $h_c^{2-D}[\mathbf{n}]$ should be a horizontal lowpass filter. Using a similar approach, the equivalent filter at the input can be expressed as follows:

$$H_{bc}^{2-D}(\boldsymbol{\omega}) = \begin{cases} H_c^{2-D}(2\omega_1 - \pi, 2\omega_2 - \pi), & i = 2 \\ H_c^{2-D}(2\omega_1 - \pi, 2^{i-1}\omega_2), & i > 2. \end{cases} \tag{7}$$

Furthermore, the spectra of $h_c^{2-D}[\mathbf{n}]$, $c[\mathbf{n}]$ and $d[\mathbf{n}]$ are similar to those illustrated in Figs. 8–10 reflected about the line $\omega_1 = \omega_2$, respectively.

The use of lowpass filtering and subtraction can be extended to the case that the split scales have different directional decomposition. First, the DFB with smaller decomposition is applied on the bandpass image in the LP. Each subband is then split into two different radial frequency bands using either a vertical or horizontal lowpass filter depending on the spectral region that the directional subband situates. As the filtering would not change the directional partitioning in the subbands, subsequent

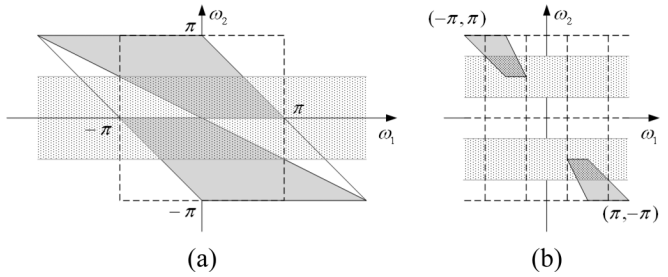

Fig. 8. Lowpass filtering for a contourlet subband: (a) response in the subband domain. (b) Response at the input of the DFB. The filter response is shown in a dot pattern.

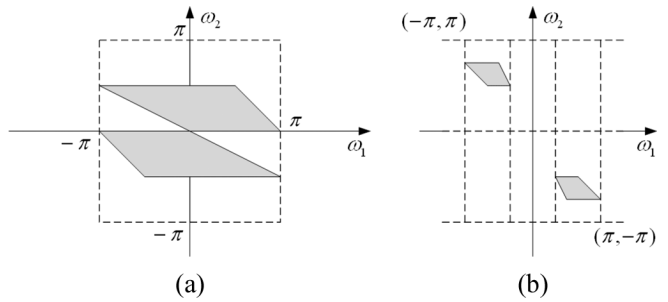

Fig. 9. Spectra of $c[\mathbf{n}]$ (a) in the subband domain and (b) at the input of the DFB.

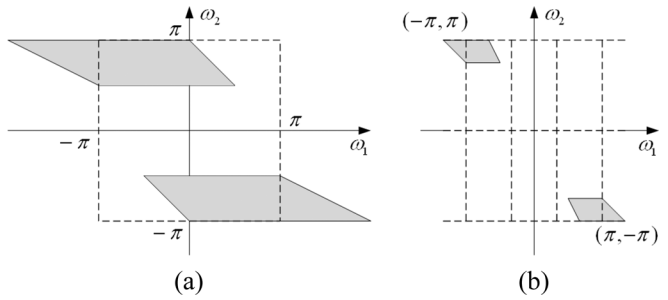

Fig. 10. Spectra of $d[\mathbf{n}]$ (a) in the subband domain and (b) at the input of the DFB.

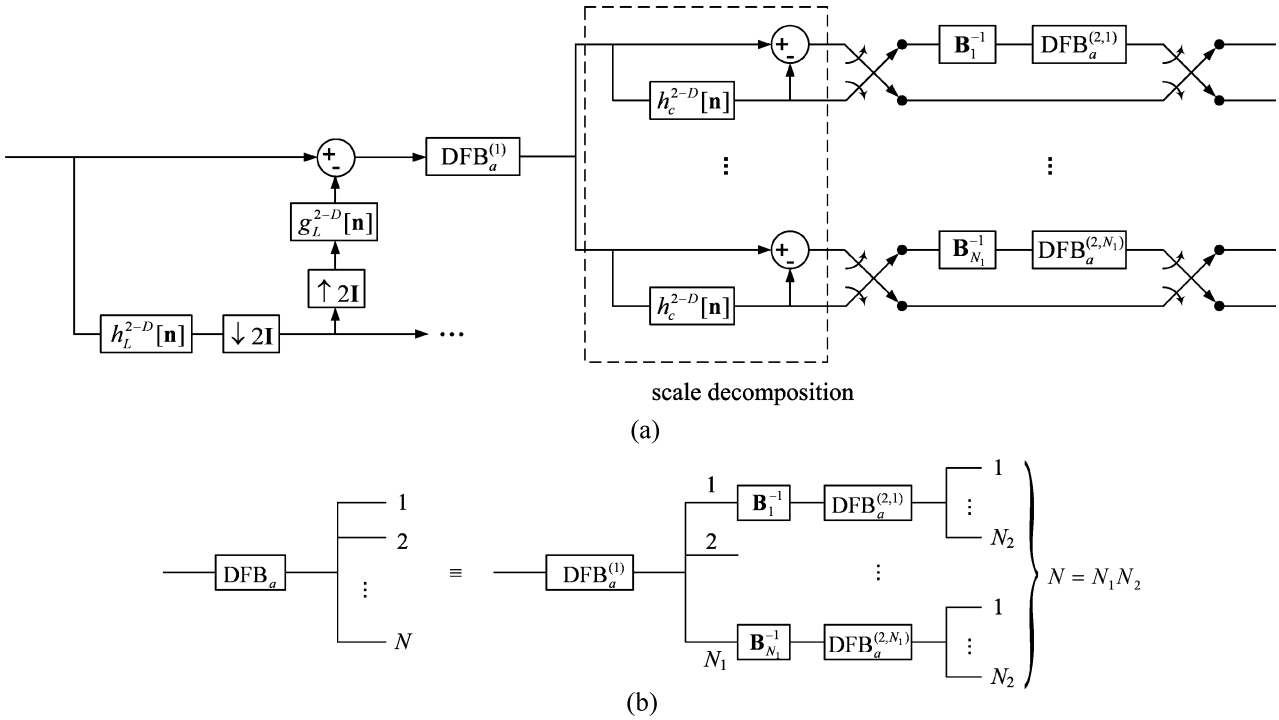

Fig. 11. (a) Proposed structure for splitting a contourlet subband into two subbands in different scales based on lowpass filtering. (b) Notations of analysis DFB stages in (a): block "DFB_a" represents an analysis DFB of larger directional decomposition among the two scales while the block "$\mathrm{DFB}_a^{(1)}$" denotes the analysis DFB of smaller directional decomposition. "$\mathrm{DFB}_a^{(2,i)}$" and "$\mathbf{B}_i^{-1}$" represent the subsequent stages of "$\mathrm{DFB}_a^{(1)}$" in "DFB_a" and inverse of backsampling for the ith subband of "$\mathrm{DFB}_a^{(1)}$." Note that all the analysis DFB blocks are incorporated with backsampling implicitly.

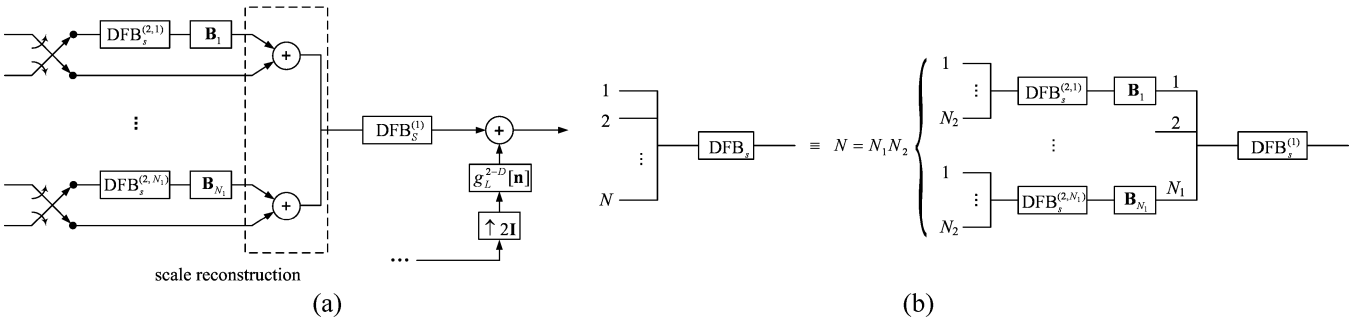

Fig. 12. (a) Synthesis structure for the proposed decomposition in Fig. 11. (b) Notations of DFB stages in (a): block "DFB_s" represents a synthesis DFB of larger directional decomposition among the two scales while the block "$\mathrm{DFB}_s^{(1)}$" denotes the synthesis DFB of smaller directional decomposition. "$\mathrm{DFB}_s^{(2,i)}$" and "$\mathbf{B}_i$" represent the previous stages of the synthesis "$\mathrm{DFB}_s^{(1)}$" in "DFB_s" and backsampling for the ith subband of "$\mathrm{DFB}_s^{(1)}$." Note that all the synthesis DFB blocks are incorporated with inverse of backsampling implicitly.

DFB stages of larger directional decomposition can be applied to the corresponding radial frequency bands after inversing the backsampling in the previous directional decomposition. As a result, different directional decompositions can be performed on the two scales. In this way, the smaller directional decomposition is shared among two scales. Fig. 11 depicts the overall decomposition scheme.

The synthesis filter banks of the proposed framework are implemented by cascading the synthesis system of subfilter banks in the reverse order of the analysis counterparts in Fig. 11. The overall structure of synthesis is shown in Fig. 12. If the basic building blocks of the DFB can perfectly reconstruct a signal, the directional subbands before scale decomposition can be reconstructed without distortion. In fact, the analysis and synthesis filter banks of the scale decomposition form a perfect reconstruction system. The synthesis signal $s_r[\mathbf{n}]$ is calculated by

$$s_r[\mathbf{n}] = c[\mathbf{n}] + d[\mathbf{n}]. \tag{8}$$

Substitute the analysis formula (3) into (8), and we have

$$s_r[\mathbf{n}] = c[\mathbf{n}] + s[\mathbf{n}] - c[\mathbf{n}] = s[\mathbf{n}]. \tag{9}$$

The above calculation also implies that the reconstruction property is independent of the lowpass filter used. Since the subsequent reconstruction of the DFB is perfect, the overall reconstruction is lossless. In the above discussion, 2-D filter $h_c^{2-D}[\mathbf{n}]$ is used. However, in the actual implementation, a 1-D filter $h_c[n]$ can be applied to each of the columns (rows) instead, if $h_c^{2-D}[\mathbf{n}]$ is a vertical (horizontal) filter.

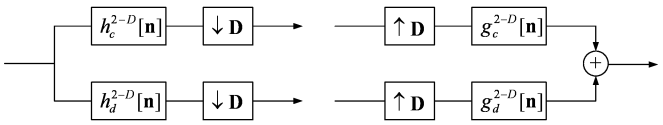

Fig. 13. Analysis and synthesis filter banks for scale decomposition based on the wavelet-like transform.

In summary, the process of lowpass filtering and subtraction provides a simple framework for splitting the contourlet subbands. Perfect reconstruction is always possible for the scale decomposition regardless of the choice of $h_c^{2-D}[\mathbf{n}]$. Furthermore, it is possible to have different directional decomposition in the two newly split scales.

C. Splitting Based on Wavelet-Like Decomposition

Besides splitting with lowpass filtering and subtraction, a wavelet-like transform can be used to decompose a subband in the contourlet transform. However, due to decimation, the directional decomposition is required to be the same in the two scales. Fig. 13 describes the decomposition scheme based on the wavelet-like transform. The subband signal $s[\mathbf{n}]$, its mid-frequency band $c[\mathbf{n}]$ and high-frequency band $d[\mathbf{n}]$ are related, respectively, by

$$c[\mathbf{n}] = \sum_{k \in Z^2} s[\mathbf{k}] h_c^{2-D}[\mathbf{Dn} - \mathbf{k}] \tag{10}$$

$$d[\mathbf{n}] = \sum_{k \in Z^2} s[\mathbf{k}] h_d^{2-D}[\mathbf{Dn} - \mathbf{k}] \tag{11}$$

where $\mathbf{D}$ is given by

$$\mathbf{D} = \begin{cases} \mathbf{D}_0, & s \text{ in } \Re_0 \\ \mathbf{D}_1, & s \text{ in } \Re_1. \end{cases} \tag{12}$$

As in the framework of Section III-B, there are either vertical or horizontal filters subject to the spectral region where the subband is located. Downsampling by a factor of 2 is then performed along the filtering direction. In reconstruction, the synthesis filter bank corresponding to the scale splitting is added to each input of the synthesis filter bank of the DFB. The overall analysis and synthesis system is similar to the system using lowpass filtering with the scale filter banks indicated by dotted lines in Figs. 11 and 12, which are to be replaced by filter banks, as shown in Fig. 13. Besides, there is no additional DFB stage for scale of larger angular resolution because the directional decomposition is assumed to be the same over the two scales. Despite that the number of subbands in the decomposed scale is doubled, the data rate in each subband is halved because of decimation so that the number of coefficients remains unchanged. It is obvious that if the DFB and the wavelet-like filter bank allow perfect reconstruction, the proposed filter bank can reconstruct the bandpass image perfectly. For FIR design, we set $G_c^{2-D}(\boldsymbol{\omega}) = H_d^{2-D}(\boldsymbol{\omega} - \mathbf{k}_1\pi)$ and $G_d^{2-D}(\boldsymbol{\omega}) = -H_c^{2-D}(\boldsymbol{\omega} - \mathbf{k}_1\pi)$, where $\mathbf{k}_1 = [1\ 0]^T$ for s in $\Re_0$ and $\mathbf{k}_1 = [0\ 1]^T$ for s in $\Re_1$ so that the aliasing components are cancelled in the reconstructed signal.

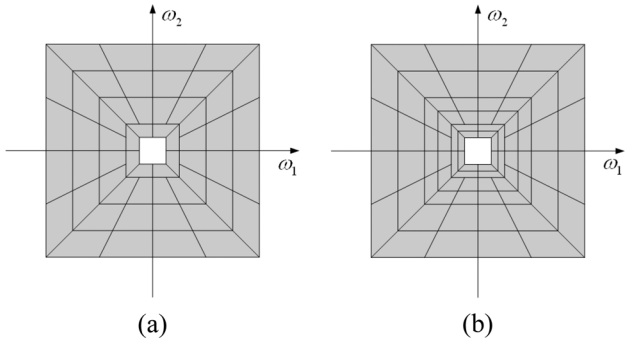

Fig. 14. Spectrum partitioning obtained by applying splitting algorithms on (a) the finest scale and (b) all scales in the contourlet transform.

For perfect reconstruction, it is further required that

$$H_c^{2-D}(\boldsymbol{\omega}) H_d^{2-D}(\boldsymbol{\omega} - \mathbf{k}_1\pi) - H_d^{2-D}(\boldsymbol{\omega}) H_c^{2-D}(\boldsymbol{\omega} - \mathbf{k}_1\boldsymbol{\pi}) = 2. \tag{13}$$

Because of efficiency, it is usually preferred to implement the 2-D filter bank by applying 1-D filter bank on each column or row. In this way, the perfect reconstruction condition has the same form as (13) with $H_c^{2-D}(\boldsymbol{\omega})$ and $H_d^{2-D}(\boldsymbol{\omega})$ replaced by their 1-D counterparts $H_c(\omega)$ and $H_d(\omega)$ and $\mathbf{k}_1 = 1$ as given in [24]. In brief, the splitting approach based on the wavelet-like transform works similar to the one based on lowpass filtering with the same directional decomposition in the two split scales. Nonetheless, the wavelet based approach can generate outputs with the same number of coefficients as the decomposed contourlet subband. The complete decomposition of MDFB, thus, possesses the same redundancy ratio as the contourlet transform, i.e., 4/3.

D. Comments on Decomposition Without Backsampling

In Section III-B and C, backsampling is always assumed. It has been shown in [25] that a backsampling matrix is a unimodular matrix, which skews a subband in spectral region $\Re_0$ in the vertical direction and a subband in spectral region $\Re_1$ in the horizontal direction. That means that the skewing direction is always perpendicular to the filtering direction of $h_c^{2-D}[\mathbf{n}]$ and $h_d^{2-D}[\mathbf{n}]$. Hence, the characteristics of the equivalent frequency response of $h_c^{2-D}[\mathbf{n}]$ and $h_d^{2-D}[\mathbf{n}]$ at the input of the DFB do not change. As a result, the proposed algorithm can still work on a directional subband at a given bandpass LP level without backsampling.

IV. Fast Algorithm for MDFB

In Section III, we have proposed two ways to split a contourlet subband into two scale components. If the splitting is applied on each scale of the contourlet transform, the frequency plane is partitioned as illustrated in Fig. 14(b). If only the finest scale is split, the same frequency partitioning of the MDFB as shown in Fig. 14(a) is achieved. In this paper, we are interested in the use of the splitting algorithms for the fast implementation of the MDFB. As the finest scale in the contourlet transform has the largest bandwidth, it should be the most effective to split the finest scale for more useful decomposition. Furthermore, the use

of nonaliasing LP as mentioned in Section II-C would broaden the bandwidth of the finest scale. This increase of bandwidth does not occur in the other coarser scales. This is because the upper end of the frequency range decreases with the lower end due to lowpass filtering in the previous level. As a result, it may not be effective for further decomposition in the coarser scale subbands as in the finest scale.

The splitting of the contourlet subbands at the finest scale using the proposed methods can reduce the complexity of the MDFB. In the original scheme, the scale decomposition is performed before the DFB is applied. Each split scale requires a single directional decomposition so in total there are two directional decompositions. However, in the new method, the directional decomposition with lower angular resolution is performed before scale decomposition. Thus, one set of operations for directional decomposition with lower angular resolution is saved by sharing. As the DFB belongs to a maximally decimated scheme, the total number of subband coefficients is the same as the size of the original image. Therefore, the scale decomposition would introduce no extra operations in contrary to the original algorithm. For separable implementation, the proposed method requires one less filtering step because it involves filtering in one direction only. If the MDFB is implemented using the decomposition method based on the wavelet-like transform described in Section III-C, the MDFB results in the same redundancy as the contourlet transform. Although it needs additional highpass filtering and downsampling, it should still be more efficient than the original method. In the subsequent analysis, the first and second approaches will be referred to fast algorithms 1 and 2, respectively. In Section IV-A, the issues of FIR filter design for the fast MDFB algorithms will be addressed. Then we show our estimation on the computational complexity in Section IV-B.

A. Filter Bank Design

Using FIR implementation, filters have no sharp transition band. Because of nonideal response, it is possible that the frequency response of a highpass filter in the proposed scheme, which extracts high-frequency components of a subband, would overlap with the lower frequency components. Denote $\omega_{\alpha p}, \omega_{\alpha s}$ and BW_α as the passband edge, stopband edge and transition bandwidth of filter $h_\alpha[n]$, where $\alpha \in \{c, d, L\}$ respectively. Note that $h_c[n]$ and $h_d[n]$ are the lowpass and highpass filters used in the proposed splitting algorithms while $h_L[n]$ is the lowpass filter adopted in the LP. The bandpass image in the LP is approximately zero in frequency $[-\omega_{\rm Lp}, \omega_{\rm Lp}]^2$ (e.g., $h_L[n]$ is a nonaliasing filter/QMF filter). Fig. 15 compares the equivalent filter response of $h_d[n]$ with the bandpass response of the LP in frequency domain at the input of the DFB. In order to avoid overlapping, it is required that

$$\omega_{\rm Lp} \geq (\pi - \omega_{ds})/2 \text{ or } \quad \text{equivalently } 2\omega_{\rm Lp} + \omega_{ds} \geq \pi. \quad (14)$$

For fast algorithm 1, (14) is equivalent to

$$2\omega_{\rm Lp} + \omega_{\rm cp} \geq \pi \quad (15)$$

because the lowpass and highpass responses are complementary to each other so that $\omega_{ds} = \omega_{\rm cp}$. Besides that, the cutoff

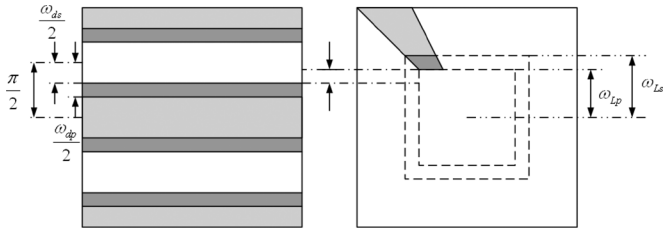

Fig. 15. (Left spectrum) Contrast of the equivalent highpass filter $h_d^{2-D}[\mathbf{n}]$ and (right spectrum) the resultant frequency response of the directional filter and the bandpass response of the LP. Note that the frequency response of the bandpass image of the LP is approximately zero in $[-\omega_{\rm Lp}, \omega_{\rm Lp}]^2$.

frequency of the lowpass filter must not be too large or too small. Otherwise, the bandwidth difference between the two split scales might be too large which in turns lower the frequency resolution. Therefore, we set the cutoff frequency of $h_c[n]$ to be $\pi/2$. In this case, $\omega_{\rm cs} = \pi - \omega_{\rm cp}$ and so $BW_c = \omega_{\rm cs} - \omega_{\rm cp} = \pi - 2\omega_{\rm cp}$. In addition to the advantage in frequency resolution, setting cutoff frequency to be $\pi/2$ allows the use of a halfband filter which has one polyphase component of one coefficient only [23]. As a result, about half of the computational time can be saved. Examples 1 and 2 about the filter bank design have been worked out based on different additional considerations. For fast algorithm 2, a filter bank design based on QMF filters [26] will be given in example 3.

Example 1—Aliasing LP: For aliasing LP, $h_L[n]$ usually has $\omega_{\rm Lp} \geq 2\pi/5$ (e.g., QMF13 and ER13 used in [19]) This implies $2\omega_{\rm Lp}+\omega_{\rm cp} \geq 4\pi/5+\omega_{\rm cp}$. If $\omega_{\rm cp} \geq \pi/5$, (15) is satisfied. Using the Parks–McClellan algorithm [27], we design an equiripple $h_c[n]$ such that $\omega_{\rm cp} = 3\pi/10$ and $\omega_{\rm cs} = 7\pi/10$, so (15) is satisfied. It is found that ripple magnitude equal to 45 dB can be achieved if the filter length is 13.

Example 2—Nonaliasing LP: To avoid aliasing in the LP, it requires the stopband edge of $h_L[n]$, $\omega_{\rm Ls} \leq \pi/2$. Let us set $\omega_{\rm Ls} = \pi/2$. Besides condition (15), $BW_c = BW_L$ is imposed. It requires that

$$\pi - 2\omega_{\rm cp} = \omega_{\rm Ls} - \omega_{\rm Lp} = \pi/2 - \omega_{\rm Lp} \Rightarrow 2\omega_{\rm cp} - \omega_{\rm Lp} = \pi/2. \quad (16)$$

Considering both (15) and (16), we have

$$\omega_{\rm cp} \geq 2\pi/5 \quad \text{and} \quad \omega_{\rm Lp} = 2\omega_{\rm cp} - \pi/2. \quad (17)$$

In order to satisfy the criteria, equiripple $h_c[n]$ with $\omega_{\rm cp} = 2\pi/5$ and $\omega_{\rm cs} = 3\pi/5$ and $h_L[n]$ with $\omega_{\rm Lp} = 3\pi/10$ and $\omega_{\rm Ls} = \pi/2$ are designed. For length 23, the ripple magnitudes of $h_c[n]$ and $h_L[n]$ are 42 and 41 dB, respectively. It should be noted that only the first bandpass image in the LP is decomposed. Therefore, $h_L[n]$ is required to satisfy the given criteria in the first level only. For other levels, other nonaliasing filters of shorter length, e.g., binomial filter of length 7 (binom7), can be used.

Example 3—Fast Algorithm 2: $h_L[n]$ can be designed to be an equiripple filter while $h_c[n]$ and $h_d[n]$ form a QMF filter pair. Due to power complementary property of QMF filters, $\omega_{ds} = \omega_{\rm cp}$ still holds as in the case of fast algorithm 1. Therefore, similar designs in examples 1 and 2 can be used. For nonaliasing LP, we design a lowpass QMF filter $h_c[n]$ with $\omega_{\rm cs} = 2\pi/5$ using a

method in [28]. The filter has length 28 with peak ripple magnitude in stopband equal to 39 dB. Then $h_d[n] = h_c[-n]$. $h_L[n]$ designed in example 2 can be re-used in this example. Same as example 2, this filter is used in the first level of LP only while another nonaliasing filter of shorter length, binom7, is used for the remaining levels in order to reduce computational load.

B. Estimation of Computational Complexity

Computational complexity can be measured in terms of the number of arithmetic operations. Without loss of generality, we estimate the number of multiplications because filter banks require similar number of additions and multiplications. The filter banks considered are constructed in polyphase structures, which use separable filtering. In particular, the DFB is implemented in a ladder structure [29]. To simplify our discussion, all polyphase components of prototype filters used are assumed to have the same length M. Define C_{OMDFB}, C_{FMDFB1} and C_{FMDFB2} to be the number of multiplications in the original algorithm of the MDFB, fast algorithms 1 and 2, respectively. For an N-pixel image, the original MDFB requires $4\mathrm{MN}$ multiplications in the first scale decomposition. The generated lowpass image still has N points so the bandpass image at the ith level in the LP consists of $N/4^{i-1}$ points. The number of multiplications used in the ith LP level is $3\mathrm{MN}/4^{i-1}$. For a N_i-point signal, the DFB requires $2D_i\mathrm{MN}_i$ for 2^{D_i} orientations. In this paper, the number of levels in the DFB is decremented by one for every two coarser levels in the LP as suggested in [7], [8]. Suppose that there are D_0 DFB levels for the initial scale. We obtain the following estimation of C_{OMDFB}:

$$\begin{aligned} C_{\mathrm{OMDFB}} &= 4\mathrm{MN}+2\mathrm{MND}_0 \\ &\quad +\sum_{i=1}^{S-1}\left(3\mathrm{MN}+2\left(D_0-\lfloor(i-1)/2\rfloor\right)\mathrm{MN}\right)/4^{i-1} \\ &\approx (8+14D_0/3)\mathrm{MN}. \end{aligned} \tag{18}$$

For our first proposed splitting algorithm, if a halfband filter is used, MN multiplications are required. The complexity is the same for the second proposed splitting algorithm if a QMF filter is used. Together with the analysis at the beginning of Section IV, C_{FMDFB1} and C_{FMDFB2} are, thus, given by

$$\begin{aligned} C_{\mathrm{FMDFB1}} &= C_{\mathrm{FMDFB2}} = C_{\mathrm{OMDFB}} - 2\mathrm{MND}_0 - 3\mathrm{MN} \\ &\approx (5+8D_0/3)\mathrm{MN}. \end{aligned} \tag{19}$$

Let us denote r_1 and r_2 as the percentages of reduction in the computational complexity using fast algorithms 1 and 2 as compared to the original MDFB, respectively. Using (18) and (19), we have

$$r_1 = r_2 = \frac{C_{\mathrm{OMDFB}} - C_{\mathrm{FMDFB2}}}{C_{\mathrm{OMDFB}}} = \frac{9+6D_0}{24+14D_0} \times 100\%. \tag{20}$$

For $D_0 = 3$, $r_1 = r_2 = 40.9\%$. Apart from number of operations, the actual running time of the algorithms has been evaluated. They are given in Section V together with further discussion on the computational complexities.

V. Experiments and Discussion

Simulation results have been performed to evaluate the actual computational time and retrieval performance of the two proposed algorithms. For comparison purpose, results for the original MDFB and the contourlet transform are included. Their implementations are based on nonaliasing LPs because aliasing would deteriorate the angular resolution. The number of directions in the scales follows the construction rule given in [7], [8] that the number of directions is halved for each two coarser levels in the LP. It should be noted that the construction rule may not be optimal for all applications other than image compression [8], [19], and it is used for comparison purpose only.

In the computational time experiment, the algorithms, which are implemented in Matlab 6.5, are performed on Lena image of size 512×512 in a computer with CPU of Intel Pentium 4 2.4 GHz. The retrieval experiments were performed on a database derived from Brodatz album [30]. The central part of each of the 111 album images of size 512×512 was extracted. It was then divided into nine 128×128 regions. As a result, the database has 999 images of 111 different classes. Each image in the database was selected once as a query image. The first nine images closest to the query image were returned from the retrieval system and used to calculate the retrieval accuracy. The mean of retrieval accuracies of all query images was used for evaluation. In feature extraction, L1 norm of the subbands excluding the lowpass one are calculated. For subband $s_i[\mathbf{n}]$, it is given by

$$f_i = \sum_{\mathbf{n}} \left|s_i[\mathbf{n}]\right|. \tag{21}$$

Since the contourlet transform and the MDFBs have different number of subbands, greedy algorithm is applied to obtain an optimal set of features for a given number of features. The distance between two texture images T_1 and T_2 was calculated using weighted sum of absolute difference [2], i.e.,

$$d(T_1, T_2) = \sum_i \left|\frac{f_i^{(1)} - f_i^{(2)}}{\sigma_i}\right| \tag{22}$$

where σ_i is the standard deviation of the selected feature f_i over the entire database and the superscript of features denotes the texture index.

Table I shows the computational time in seconds while the percentages of reduction in the computational time together with the estimated reduction in complexity in Section IV-B is given in Table II. From Table I, it can be seen that the two proposed algorithms always use less time as compared with the original algorithm. The percentages of reduction in computational time of the proposed algorithms are between 33.3%–37.5% for both of fast algorithm 1 and fast algorithm 2 as compared to the original MDFB algorithm. Our estimation given in Section IV-B agrees roughly with the experimental results with some variations. The variations partly attribute to the assumption that all polyphase components of filters have the same length. Another reason is that besides arithmetic operations, there are other operations such as memory access in sampling, etc. Despite this, both of them show considerable reduction in computational complexity which mainly comes from the saving of directional decomposition on the finest bandpass

TABLE I
COMPUTATIONAL TIME IN SECOND FOR THE PROPOSED FAST ALGORITHMS AND THE ORIGINAL ALGORITHM OF THE MDFB AND THE CONTOURLET TRANSFORM

Decomposition of MDFB / Contourlet [b]	Fast algorithm 1	Fast algorithm 2	Original MDFB	Contourlet
(3-3, 3, 2) / (3, 3, 2)	1.69	1.62	2.59	1.38
(4-4, 4, 3) / (4, 4, 3)	1.98	1.87	2.97	1.61

[a] Fast algorithms 1 and 2 are implemented as in examples 2 and 3 given in Section IV-A, respectively. The LP and DFB in the original algorithm MDFB and the contourlet transform are implemented in the same way as in the fast algorithms. For the original MDFB algorithm, the decomposition of the finest scale is achieved using 2-D separable filtering based on an equiripple filter of length 17.

[b] For MDFB algorithms, decomposition $(d_{11} - d_{12}, d_2, d_3)$ refers to the MDFB in which d_{11} and d_{12} levels directional decompositions are performed for the first and second scales split from the finest bandpass image in the LP, respectively, while d_2 levels and d_3 levels directional decompositions are performed in the second and third bandpass images in the LP respectively. For the contourlet transform, decomposition (d_1, d_2, d_3) refers to the contourlet transform with d_i level decomposition on the ith bandpass image in the LP, $i = 1$, 2, and 3.

TABLE II
PERCENTAGE OF REDUCTION IN COMPUTATIONAL TIME AND NUMBER OF MULTIPLICATIONS FOR THE PROPOSED FAST ALGORITHMS

Decomposition	Fast algorithm 1	Fast algorithm 2	r_1 / r_2
(3-3, 3, 2)	34.6%	37.5%	40.9%
(4-4, 4, 3)	33.3%	37.1%	41.3%

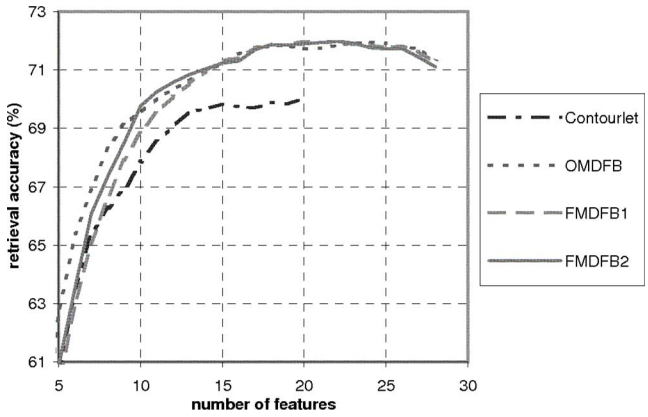

Fig. 16. Comparison of retrieval accuracy of the contourlet transform, the original MDFB algorithms (OMDFB), fast algorithm 1 (FMDFB1), and fast algorithm 2 (FMDFB2) at different number of selected features for decomposition (3-3, 3, 2)/(3, 3, 2).

image in the LP. In our estimation and implementation of fast algorithm 2, QMF filters that can be implemented in an efficient polyphase structure are considered. For general implementation, fast algorithm 2 should require more operations than fast algorithm 1 because it requires an extra bandpass filtering.

Compared with the contourlet transform, the fast algorithm uses slightly more time because of additional scale decomposition. However, this additional scale splitting allows the proposed algorithms to outperform the contourlet transform in texture retrieval. Their retrieval accuracy is plotted against number of selected features larger or equal to five in Figs. 16 and 17

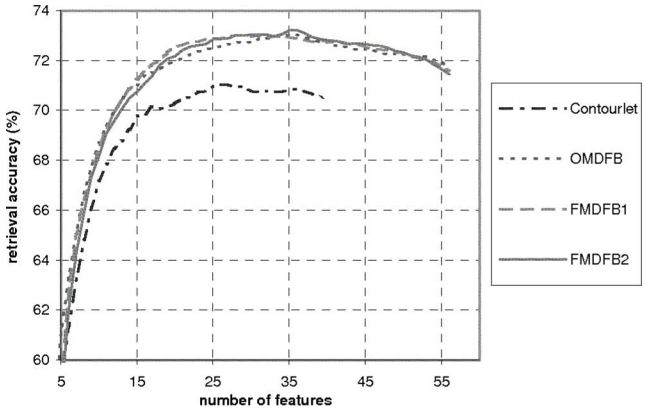

Fig. 17. Comparison of retrieval accuracy of the contourlet transform, the original MDFB algorithms (OMDFB), fast algorithm 1 (FMDFB1), and fast algorithm 2 (FMDFB2) at different number of selected features for decomposition (4-4, 4, 3)/(4, 4, 3).

for decomposition (3-3, 3, 2)/(3, 3, 2) and (4-4, 4, 3)/(4, 4, 3), respectively. The results show that the retrieval performance of the MDFB algorithms is better than the contourlet transform if more than seven features are selected. The maximum retrieval accuracy for the contourlets, which is achieved when 26 features are used, is 71.1% in the case of decomposition (4-4, 4, 3)/(4, 4, 3). However, the retrieval accuracy of fast algorithm 1 and fast algorithm 2 is both higher than that by 1.8%, respectively, for the same number of features. From the figure, we can also find that the retrieval performance of the two fast algorithms is close to that of the original MDFB algorithm. This is due to their similarity in spectrum partitioning. However, the use of the new algorithms benefits from lower complexity and also reduced redundancy for the second algorithm.

VI. CONCLUSION

We have presented two fast algorithms for MDFB, in which directional decomposition is performed prior to the scale decomposition in the first two scales. In this way, directional decomposition can be shared over the first two scales. This results in saving one directional decomposition. The first fast algorithm decomposes the bandpass directional subbands using lowpass filtering and subtraction. It permits different directional decompositions in the two scales. The second scheme utilizes wavelet-like decomposition. Although directional decomposition of the two scales is required to be the same in the second scheme, it can generate subbands with the same redundancy as the contourlet transform. Perfect reconstruction is possible if the constituent filter banks do not introduce distortion.

Several aspects of the fast algorithms have been studied. We have presented and discussed some possible FIR designs of both proposed schemes based on aliasing and nonaliasing LPs. Computational complexity of the proposed methods have been analyzed. Our results show that a reduction about 33%–37% can be achieved when compared with the original scheme. Furthermore, we have conducted texture retrieval experiments and find that the fast algorithms had nearly the same retrieval performance as the original MDFB. Thus, the same multiscale and multidirectional textural features are preserved using our two proposed fast algorithms.

The improved efficiency in the proposed fast algorithms should broaden the applications of MDFB in image processing, especially those require real time processing. The reduced redundancy of the MDFB based on the wavelet-like transform also gives great potential for image compression. Currently, we use the splitting algorithms proposed in Section III to implement the fast MDFB algorithms. We have shown in Section IV that the algorithms can be used to generate an image representation with finer scales as illustrated in Fig. 14(b). Although the large number of subbands would complicate the process of feature extraction, the effectiveness of this kind of decomposition for image representation should improve if it is associated with certain basis selection algorithms similar to wavelet packet [22]. This will be our future direction on the multiscale analysis using the DFBs.

ACKNOWLEDGMENT

The authors thank the anonymous reviewers for their constructive comments. K.-O. Cheng would like to thank the Department of Electronic and Information Engineering, The Hong Kong Polytechnic University, for the research studentship that he received.

REFERENCES

[1] S. G. Mallat, "A theory for multiresolution signal decomposition: The wavelet representation," *IEEE Trans. Pattern Anal. Mach. Intell.*, vol. 11, no. 7, pp. 674–693, Jul. 1989.

[2] B. S. Manjunath and W. Y. Ma, "Texture features for browsing and retrieval of image data," *IEEE Trans. Pattern Anal. Mach. Intell.*, vol. 18, no. 8, pp. 837–842, Aug. 1996.

[3] G. M. Haley and B. S. Manjunath, "Rotation-invariant texture classification using a complete space-frequency model," *IEEE Trans. Image Process.*, vol. 8, no. 2, pp. 255–269, Feb. 1999.

[4] W. T. Freeman and E. H. Adelson, "The design and use of steerable filters," *IEEE Trans. Pattern Anal. Mach. Intell.*, vol. 13, no. 9, pp. 891–906, Sep. 1991.

[5] E. P. Simoncelli, W. T. Freeman, E. H. Adelson, and D. J. Heeger, "Shiftable multiscale transforms," *IEEE Trans. Inf. Theory*, vol. 38, no. 2, pp. 587–607, Mar. 1992.

[6] E. P. Simoncelli and W. T. Freeman, "The steerable pyramid: A flexible architecture for multi-scale derivative computation," in *Proc. IEEE Int. Conf. Image Processing*, Oct. 1995, vol. 3, pp. 444–447.

[7] M. N. Do and M. Vetterli, "Pyramidal directional filter banks and curvelets," in *Proc. IEEE Int. Conf. Image Processing*, Oct. 2001, vol. 3, pp. 158–161.

[8] M. N. Do and M. Vetterli, "The contourlet transform: An efficient directional multiresolution image representation," *IEEE Trans. Image Process.*, vol. 14, no. 12, pp. 2091–2106, Dec. 2005.

[9] E. L. Pennec and S. Mallat, "Sparse geometric image representations with bandelets," *IEEE Trans. Image Process.*, vol. 14, no. 4, pp. 423–438, Apr. 2005.

[10] V. Velisavljevic, B. Beferull-Lozano, M. Vetterli, and P. L. Dragotti, "Directionlets: Anisotropic multidirectional representation with separable filtering," *IEEE Trans. Image Process.*, vol. 15, no. 7, pp. 1916–1933, Jul. 2006.

[11] C.-L. Chang and B. Girod, "Direction-adaptive discrete wavelet transform via directional lifting and bandeletization," in *Proc. IEEE Int. Conf. Image Process.*, Oct. 2006, pp. 1149–1152.

[12] W. Ding, F. Wu, and S. Li, "Lifting-based wavelet transform with directional spatial prediction," presented at the Picture Coding Symp., San Francisco, CA, Dec. 2004.

[13] P. J. Burt and E. H. Adelson, "The Laplacian pyramid as a compact image code," *IEEE Trans. Commun.*, vol. COM-31, no. 4, pp. 532–540, Apr. 1983.

[14] M. N. Do and M. Vetterli, "Framing pyramids," *IEEE Trans. Signal Process.*, vol. 51, no. 9, pp. 2329–2342, Sep. 2003.

[15] R. H. Bamberger and M. J. T. Smith, "A filter bank for the directional decomposition of images: Theory and design," *IEEE Trans. Signal Process.*, vol. 40, no. 4, pp. 882–893, Apr. 1992.

[16] E. J. Candes and D. L. Donoho, "Curvelets—A surprisingly effective nonadaptive representation for objects with edges," in *Curves and Surfaces Fitting*, L. L. Schumaker, Ed. *et al.* Nashville, TN: Vanderbilt Univ. Press, 1999.

[17] T. T. Nguyen, "The multiresolution directional filter banks," Ph.D. dissertation, Dept. Elect. Eng., Univ. Texas, Arlington, Aug. 2006.

[18] W. Y. Chan, N. F. Law, and W. C. Siu, "Multiscale feature analysis using directional filter bank," in *Proc. 2003 Joint Conf. 4th Int. Conf. Information, Communications, Signal Processing, 4th Pacific Rim Conf. Multimedia*, Dec. 2003, vol. 2, pp. 822–826.

[19] K. O. Cheng, N. F. Law, and W. C. Siu, "Multiscale directional filter bank with applications to structured and random texture retrieval," *Pattern Recognit.*, vol. 40, no. 4, pp. 1182–1194, Apr. 2007.

[20] S.-I. Park, M. J. T. Smith, and R. M. Mersereau, "A new directinal filter bank for image analysis and classification," in *Proc. IEEE Int. Conf. Acoust., Speech, Signal Process.*, Mar. 1999, vol. 3, pp. 1417–1420.

[21] S.-I. Park, M. J. T. Smith, and R. M. Mersereau, "Improved structures of maximally decimated directional filter banks for spatial image analysis," *IEEE Trans. Image Process.*, vol. 13, no. 11, pp. 1424–1431, Nov. 2004.

[22] T. Chang and C.-C. J. Kuo, "Texture analysis and classification with tree-structured wavelet transform," *IEEE Trans. Image Process.*, vol. 2, no. 4, pp. 429–441, Oct. 1993.

[23] P. P. Vaidyanathan, *Multirate Systems and Filter Banks*. Englewood Cliffs, NJ: Prentice-Hall, 1993.

[24] M. Vetterli and C. Herley, "Wavelet and filter banks: Theory and design," *IEEE Trans. Signal Process.*, vol. 40, no. 9, pp. 2207–2232, Sep. 1992.

[25] M. N. Do, "Directional multiresolution image representations," Ph.D. dissertation, School Comput. Commun. Sci., Swiss Fed. Inst. Technol., Lausanne, Switzerland, 2001.

[26] D. Esteban and C. Galand, "Application of quadrature mirror filters to split band voice coding schemes," in *Proc. IEEE Int. Conf. Acoust., Speech, Signal Processing*, May 1977, vol. 2, pp. 191–195.

[27] J. H. McClellan, T. W. Parks, and L. R. Rabiner, "FIR linear phase filter design program," in *Programs for Digital Signal Processing*. New York: IEEE Press, 1979, pp. 5.1-1–5.1-13, The Digital Signal Processing Committee, IEEE Acoustics, Speech, and Signal Processing Society (Eds.).

[28] C.-K. Chen and J.-H. Lee, "Design of quadrature mirror filters with linear phase in the frequency domain," *IEEE Trans. Circuits Syst. II, Exp. Briefs*, vol. 39, no. 9, pp. 593–605, Sep. 1992.

[29] S.-M. Phoong, C. W. Kim, P. P. Vaidyanathan, and R. Ansari, "A new class of two-channel biorthogonal filter banks and wavelet bases," *IEEE Trans. Signal Process.*, vol. 43, no. 3, pp. 649–665, Mar. 1995.

[30] P. Brodatz, *Texture: A Photographic Album for Artists and Designers*. New York: Dover, 1966.

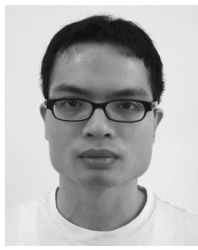

Kin-On Cheng received the B.Eng. degree (first-class honours) and M.Phil. degree in electrical and electronic engineering from The Hong Kong University of Science and Technology, Hong Kong, 2001 and 2003, respectively. He is currently pursuing the Ph.D. degree at The Hong Kong Polytechnic University.

His research interests include signal processing, texture classification, and bioinformatics.

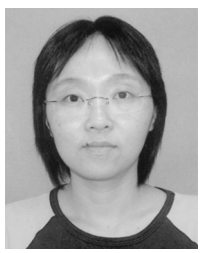

Ngai-Fong Law (M'94) received the B.Eng. degree with first-class honors from the University of Auckland, New Zealand, in 1993, and the Ph.D. degree from the University of Tasmania, Australia, in 1997, both in electrical and electronic engineering.

She is currently an Assistant Professor in the Electronic and Information Engineering Department, Hong Kong Polytechnic University, Hong Kong. Her research interests include wavelet transform, pattern recognition, and bioinformatics.

Wan-Chi Siu (S'77–M'77–SM'90) received the Associateship from The Hong Kong Polytechnic University, Hong Kong, the M.Phil. degree from The Chinese University of Hong Kong in 1975 and 1977, respectively, and the Ph.D. Degree from the Imperial College of Science, Technology and Medicine, London, U.K., in October 1984.

He was with The Chinese University of Hong Kong as a Tutor and later as an Engineer between 1975 and 1980. He then joined The Hong Kong Polytechnic University as a Lecturer in 1980. He was promoted to Senior Lecturer, Principle Lecturer, and Reader in 1985, 1987, and 1990, respectively, and has been Chair Professor of the Department of Electronic and Information Engineering since 1992. He was Head of Department of Electronic and Information Engineering Department and subsequently Dean of Engineering Faculty between 1994 and 2002. He is currently the Director of the Centre for Multimedia Signal Processing of the same university. He has published 300 research papers, over 130 of which appeared in international journals, such as the IEEE TRANSACTIONS ON SIGNAL PROCESSING, and he is an Editor of the recent book *Multimedia Information Retrieval and Management* (Springer, 2003). His research interests include digital signal processing, fast computational algorithms, transforms, wavelets, image and video coding, and computational aspects of pattern recognition.

Prof. Siu was a Guest Editor, Associate Editor, and Editorial Board Member of the IEEE TRANSACTIONS ON CIRCUITS AND SYSTEMS—II: PATTERN RECOGNITION, the *Journal of VLSI Signal Processing Systems for Signal, Image, Video Technology*, the *EURASIP Journal on Applied Signal Processing*, in addition to other journals. He has been a keynote speaker at many international conferences, including IEEE PCM 2002 (Taiwan, R.O.C.) and the IEEE 2003 ICNNSP (Nanjing, China). He has held the position of General Chair or Technical Program Chair of many international conferences, including IEEE Society sponsored flagship conferences such as ISCAS 1997, ICASSP 2003, and ICIP 2010 (to be held in Hong Kong). Between 1991 and 1995, he was a member of the Physical Sciences and Engineering Panel of the Research Grants Council (RGC), Hong Kong Government, and in 1994, he chaired the first Engineering and Information Technology Panel of the Research Assessment Exercise (RAE) to assess the research quality of 19 Cost Centers (departments) from all universities in Hong Kong. He has received many awards, including the Distinguished Presenter Award (1997), the IEEE Third Millennium Medal (2000), the Best Teacher Award (2003), the Outstanding Award in Research (2003), the Plaque for Exceptional Leadership from IEEE SPCB (2003), and an Honorable Mention Winner Award from Pattern Recognition (2004).